Immunofibroblasts are pivotal drivers of tertiary lymphoid structure formation and local pathology

Saba Nayar[a,b,1], Joana Campos[a,b,1], Charlotte G. Smith[a,b], Valentina Iannizzotto[a,b], David H. Gardner[a,b], Frédéric Mourcin[c], David Roulois[c], Jason Turner[a,b], Marvin Sylvestre[c], Saba Asam[a,b], Bridget Glaysher[d], Simon J. Bowman[a,b], Douglas T. Fearon[e], Andrew Filer[a,b], Karin Tarte[c], Sanjiv A. Luther[f], Benjamin A. Fisher[a,b], Christopher D. Buckley[a,b,2], Mark C. Coles[d,2,3], and Francesca Barone[a,b,3]

[a]Rheumatoid Arthritis Pathogenesis Centre of Excellence, Institute of Inflammation and Ageing, College of Medical & Dental Sciences, University of Birmingham Research Laboratories, Queen Elizabeth Hospital, B15 2WB Birmingham, United Kingdom; [b]NIHR Birmingham Biomedical Research Centre, University Hospitals Birmingham NHS Foundation Trust, University of Birmingham, B15 2TT, Birmingham, UK; [c]UMR INSERM U1236, Université Rennes 1, Etablissement Français du Sang, 35043 Rennes, France; [d]Centre for Immunology and Infection, Department of Biology, Hull York Medical School, University of York, YO10 5DD York, United Kingdom; [e]Cancer Research UK Cambridge Institute, Li Ka Shing Centre, University of Cambridge, CB2 0RE Cambridge, United Kingdom; and [f]Department of Biochemistry, Center of Immunity and Infection, University of Lausanne, 1066 Epalinges, Switzerland

Resident fibroblasts at sites of infection, chronic inflammation, or cancer undergo phenotypic and functional changes to support leukocyte migration and, in some cases, aggregation into tertiary lymphoid structures (TLS). The molecular programming that shapes these changes and the functional requirements of this population in TLS development are unclear. Here, we demonstrate that external triggers at mucosal sites are able to induce the progressive differentiation of a population of podoplanin (pdpn)-positive stromal cells into a network of immunofibroblasts that are able to support the earliest phases of TLS establishment. This program of events, that precedes lymphocyte infiltration in the tissue, is mediated by paracrine and autocrine signals mainly regulated by IL13. This initial fibroblast network is expanded and stabilized, once lymphocytes are recruited, by the local production of the cytokines IL22 and lymphotoxin. Interfering with this regulated program of events or depleting the immunofibroblasts in vivo results in abrogation of local pathology, demonstrating the functional role of immunofibroblasts in supporting TLS maintenance in the tissue and suggesting novel therapeutic targets in TLS-associated diseases.

fibroblasts | Sjögren's syndrome | autoimmunity | tertiary lymphoid structures

The establishment of TLS (tertiary lymphoid structures) is a phenomenon associated with cancer, infection, and autoimmunity (1). Within peripheral tissue, in autoimmune conditions such as primary Sjögren's syndrome (pSS), TLS form pathogenic hubs of acquired immune responses that are classically associated with a Th2 paradigm, ectopic autoantibody production, and the potential expansion of malignant autoreactive B cell clones (1).

While principally composed of lymphocytes and dendritic cells, TLS organization is supported by a complex network of nonhematopoietic stromal cells. These include endothelial cells, lymphatic vessels, nerves, and immunofibroblasts that closely resemble the fibroblastic reticular cells (FRCs) that inhabit secondary lymphoid organs (SLOs). These populations form a network that is believed to support the organization and maintenance of the immune cells in TLS and have been deemed responsible for local disease resistance to lymphocyte depletion (2, 3).

Elegant in vivo and in silico studies have revealed the heterogeneity of the stromal cell populations in SLOs (4) and demonstrated that interfering with the podoplanin (pdpn)[+]/Fibroblast activation protein 1 (FAP)[+] network of immunofibroblasts profoundly affects immune cell homeostasis (5–7). Similar data are not available in chronic autoimmune conditions where targeting the pathogenic microenvironment could be envisaged, alongside immune-cell biological therapy, to induce disease remission.

During embryogenesis, innate lymphoid cells (ILCs) provide molecular cues for the activation of the resident mesenchyme in ICAM-1^{high}, VCAM-1^{high} organizer cells (8–10). Thereafter,

lymphocyte migration in the anlagen is responsible for the full differentiation of FRCs within distinct areas of an SLO. Within TLS, the molecular requirement for immunofibroblast specification is still debated (2), and this hampers the development of therapeutics aimed at targeting this population in humans.

We and others have previously demonstrated that specific cytokines might support the acquisition of pathogenic features of resident fibroblasts (11–15). However, a broader understanding of the signals involved in TLS mesenchymal specification is still missing, and definitive proof that targeting activated fibroblasts might interfere with TLS-associated disease is not available.

Here, we provide evidence that immunofibroblasts in human and murine TLS are required to support local pathology and support the production of antinuclear antibodies (ANAs). We show that human TLS are underpinned by the formation of a network of

Significance

TLS, which are clusters of lymphocytes and stromal cells observed at sites of chronic inflammation, play a key role in sustaining disease progression in autoimmune conditions. While the role of lymphocytes in these structures has been studied extensively, the role of fibroblasts, nonhematopoietic stromal cells, in the formation and maintenance of TLS has not been demonstrated. Here, we establish that, at sites of TLS establishment, resident fibroblasts expand and acquire immunological features in a process that is dependent on IL13 and IL22. Interference with this process or depletion of immunofibroblasts leads to involution of TLS, resulting in decreased immune-cell activation and resolution of tissue pathology, thus supporting the use of fibroblast-targeting strategies to treat TLS-associated autoimmune diseases.

Fig. 1. TLS human fibroblasts are characterized by expression of pdpn, FAP, and adhesion molecules. (A) Immunofluorescence analysis of salivary gland biopsy from pSS patient stained for pdpn (red), FAP (green), and DAPI (blue). (Scale bar: 250 μm.) (B) viSNE plots of CD45−CD235a−CD11b−EpCAM−CD31− cells from pSS patients' salivary gland biopsy tissue, analyzed by multicolor flow cytometry. Colors indicate cell expression level of labeled markers (pdpn, FAP, ICAM-1, and VCAM-1). (C) Principle component analysis (PCA) plot from pdpn+ single-cell PCR data. Data are shown for FAP, ICAM-1, VCAM-1, and CD34 in the 2 clusters identified by hierarchical clustering analysis. (D) viSNE plots of CD45−CD235a−CD11b−EpCAM−CD31− cells from pSS patients' salivary gland biopsy tissue, analyzed by multicolor flow cytometry. Colors indicate cell expression level of labeled markers (CD34). Graphs show differential gene expression data for baff, il7, pdgfrα, cxcl12, pdgfrβ, cxcl13, ccl19, ccl21, il4rα, and il22rα transcripts in FACS-sorted CD34+ and CD34−pdpn+ populations. Data are expressed as mean ± SD ($n = 5$); *$P < 0.05$; **$P < 0.01$; paired t test. (E) Expression of *vcam1*, *icam1*, and *pdpn* mRNA transcript levels in pSS fibroblasts stimulated in vitro with IL13, TNF, and LTα1β2 ($n = 5$). Relative quantitation (RQ) was calculated with unstimulated cells. *$P < 0.05$; **$P < 0.01$; one-way ANOVA. Data are represented as mean ± SD. (F) Analysis of the percentage of pSS fibroblasts positive for BrdU flow cytometry staining post in vitro stimulation with IL22, TNF, and LTα1β2 ($n = 5$). *$P < 0.05$; one-way ANOVA. Data are represented as mean ± SD.

immunofibroblasts that express pdpn and FAP and respond in vitro to stimulation with Th2 cytokines and IL22. In vivo, we demonstrate the presence of resident immunofibroblast progenitors at the sites of TLS establishment, whose development is initiated by IL13. We prove that leukocytes are dispensable for this early phase of priming but are later required for the expansion of the fibroblast network, in a process mediated by the expression of IL22 and LTα1β2. Finally, we show that targeting this microenvironment in vivo, either by depleting immunofibroblasts or interfering with their cytokine-dependent developmental pathway, is sufficient to induce abrogation of local pathology and silence the humoral autoantibody response. As such, we provide evidence that targeting immunofibroblasts, alongside lymphocytes, could be considered to achieve long-term remission in chronic inflammatory diseases.

Results

IL13 and IL22 Modulate the Phenotype and Proliferation of the TLS Immunofibroblasts in Salivary Glands of Patients with pSS.

The establishment of TLS in the salivary glands of patients with pSS is supported by a fibroblast network that express pdpn and FAP, identified both by immunofluorescence (Fig. 1*A* and *SI Appendix*, Fig. S1) and flow cytometry (Fig. 1*B*). The development of this network in human samples, that is similar to the FRC network observed in the SLOs (16), correlates with the severity of CD45^{+} immune cell infiltration (*SI Appendix*, Fig. S1). Single-cell PCR analysis of the pdpn^{+} fibroblasts unveiled 2 separate clusters (1, 2). Cluster 1 was characterized by enrichment for FAP, ICAM-1, VCAM-1, and CD34 transcripts (Fig. 1*C*). Given the overlap between CD34 and ICAM-1/VCAM-1 expression, CD34 was used as a surrogate marker to sort CD34^{+} and CD34-PDPN^{+} cells, the former being ICAM^{high}/VCAM^{high} (*SI Appendix*, Fig. S1). Interestingly, sorted pdpn^{+}CD34^{+} cells display enrichment for transcripts encoding for IL7 and B cell activation factor (BAFF) while pdpn^{+}CD34^{-} cells showed enrichment for transcripts encoding for CXCL13, CCL19, and CCL21 (Fig. 1*D*). These data suggest that, within the pdpn^{+} population in humans, 2 subpopulations of stromal cells are present that respectively support lymphocyte survival and organization within the TLS. Both populations were found to express receptors for TNFα, LTα1β2, IL4, and IL13, and for IL22, a cytokine that we previously demonstrated to be responsible for chemokine expression in TLS (12) (Fig. 1*D* and *SI Appendix*, Fig. S1).

IL13 expression has been previously associated with autoimmunity (17–22). Interestingly, the in vitro challenge of human isolated fibroblasts with IL13 significantly increased the expression of VCAM-1 and, to a lesser extent, pdpn and ICAM-1 in synergy with TNFα and LTα1β2 (Fig. 1*E*). On the contrary, stimulation of the same fibroblasts with IL22 demonstrated the functional ability of this cytokine to induce cell proliferation (Fig. 1*F*). However, IL22 did not induce VCAM-1, ICAM-1, and pdpn (*SI Appendix*, Fig. S1). While a certain degree of variability was observed in the fibroblasts' response to cytokines in vitro, our results suggested the possibility that cytokines belonging to different families exert different and complementary effects on the resident mesenchyme and cooperate with the TNFα family members toward the acquisition of an immune-pathogenic phenotype during TLS assembly.

Immunofibroblast Activation and Expansion Are Observed During TLS Formation in a Murine Model of Induced Salivary Gland Inflammation.

We took advantage of a previously described model of TLS assembly, characterized by formation of TLS upon salivary gland infection of wild-type (wt) mice with AdV5 (10^{8-12} plaque-forming unit) (23). We demonstrated that progressive lymphocyte aggregation in the salivary glands upon infection (*SI Appendix*, Fig. S2) is underpinned by the expansion of a network of (CD45^{-}EPCAM^{-}CD31^{-}) pdpn^{+} fibroblasts which are similar to those observed in humans and precedes lymphocyte infiltration and reverts to

baseline levels upon clearance of the TLS from the tissue (Fig. 2 *A* and *B* and *SI Appendix*, Fig. S2). This population is characterized by expression of additional stromal cell markers, such as pdgfrα and pdgfrß, FAP, ICAM-1, VCAM-1, MadCAM, and RANK-L (Fig. 2*C* and *SI Appendix*, Fig. S2). Pdpn[+] fibroblasts were found to express CXCL13, CCL19, BAFF, IL7, and LTβR (Fig. 2*D* and *SI Appendix*, Fig. S2). Interestingly, subdividing the pdpn[+] population into ICAM-1^{+}/VCAM-1^{+} or ICAM-1^{+}VCAM-1^{-} and ICAM-1^{-}/VCAM-1^{+} unveiled increased expression of lymphoid chemokines, but not survival factors in the ICAM-1^{+}/VCAM-1^{+} (double positive) pdpn[+] fibroblasts (Fig. 2*E*).
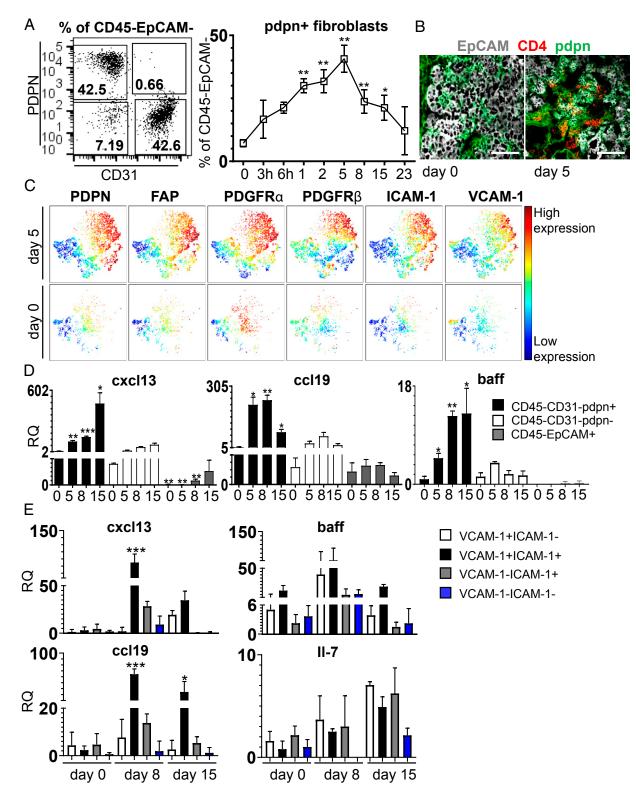
All together, these data demonstrate that the expression of pdpn identifies within both human and murine TLS a heterogeneous population of immunofibroblasts that are able to support the key immunological functions of survival and migration/organization exerted in the SLOs by FRCs (*SI Appendix*, Fig. S2). As demonstrated in human TLS fibroblasts, pdpn[+] fibroblasts are characterized by the expression of IL4R, IL13R, and, as previously described, of IL22R (12), alongside TNFR and LTβR (*SI Appendix*, Fig. S2) (12).

IL4R Engagement Regulates Stromal Cell Priming in an Animal Model of TLS Assembly.

To dissect in vivo the role of these receptors in TLS assembly, we induced salivary gland inflammation in mice deficient for IL4R, IL4, and IL13. We demonstrated that, in vivo, the deficiency of IL4R or IL13, but not of IL4, resulted in a failure to up-regulate pdpn[+] and to prime resident progenitors (Fig. 3*A* and *SI Appendix*, Fig. S3). Interestingly, this defect was not accompanied by defective stromal cell proliferation (*SI Appendix*, Fig. S3). Instead, IL4R^{−/−} mice displayed defective TLS assembly, including decreased production of homeostatic chemokines (Fig. 3*B*) and formation of smaller inflammatory foci in the salivary glands (Fig. 3*C*). While chemokine expression was compensated in the absence of IL4R signaling by day 15 post-infection, autoantibody production was, in the IL4R^{−/−}, completely abolished (*SI Appendix*, Fig. S3).

To understand the relevance of IL13 in wild type (wt) animals, we investigated the expression of this cytokine upon salivary glands following viral infection in C57/bl6 mice. A rapid induction of IL13, but not of IL4, was observed in these animals in the early phases of TLS formation (Fig. 3*C*). IL13^{+} cells were localized in the inner part of the developing TLS in C57/bl6 mice reconstituted with IL13gfp bone marrow (Fig. 3*D*). Innate lymphoid cells were identified as an early source of IL13 (Fig. 3*E*), alongside fibroblasts and epithelial cells (Fig. 3*F* and *SI Appendix*, Fig. S3). This was confirmed by mixed bone marrow chimera experiments that demonstrate the conserved ability of mice reconstituted with IL13gfp bone marrow (deficient for IL13 in the hematopoietic compartment) to prime resident fibroblasts (*SI Appendix*, Fig. S3). Together, these data confirm that priming of the resident progenitors occurs independently of lymphocyte infiltration in the TLS and that IL13, but not IL4, is responsible for the early engagement of the IL4R signaling on the immunofibroblast progenitors. To test this hypothesis, we delivered recombinant IL13 (rIL13) into murine salivary glands in vivo, and we found that IL13 alone was able to induce up-regulation of pdpn, ICAM-1, and VCAM-1 (*SI Appendix*, Fig. S3).

Immunofibroblast Proliferation Is Dependent on IL22/IL22R Interaction.

Observations in wt mice demonstrated that the pdpn[+] fibroblasts undergo a phase of active proliferation after priming (*SI Appendix*, Fig. S4); however, this is not regulated by IL13 or IL4. We therefore aimed to investigate the molecular mechanism underpinning this phenomenon.

We previously demonstrated that IL22 regulates CXCL13 expression in TLS (12). Moreover, human fibroblasts isolated from pSS salivary glands expand in vitro in response to IL22, suggesting the possibility that this cytokine also mediates fibroblast proliferation in vivo, during TLS assembly. Murine fibroblasts

Fig. 2. Salivary gland inflammation induces activation and expansion of pdpn+ fibroblasts in murine salivary glands. (*A*) Representative flow cytometry plot of pdpn+ cells within CD45−EpCAM− cells and time course analysis of percentage of pdpn+ fibroblasts in wt mice. Data are presented as mean ± SD of 3 independent experiments with at least four biological replicates. *$P < 0.05$; **$P < 0.01$; one-way ANOVA. (*B*) Immunofluorescence staining for EpCAM (gray), CD4 (red), and pdpn (green) in salivary glands at days 0 and 5 p.c. (Scale bars: 100 μm.) (*C*) Representative viSNE plots of CD45− EpCAM−CD31− cells from salivary glands at days 0 and 5 p.c., analyzed by multicolor flow cytometry. Colors indicate cell expression level of labeled markers (pdpn, FAP, PDGFRα, PDGFRβ, ICAM-1, and VCAM-1). (*D*) Gene expression analysis for cxcl13, baff, ccl19, and il7 transcripts on sorted populations (pdpn+ fibroblasts, pdpn− fibroblasts, and EpCAM+ cells). Relative quantitation (RQ) was calculated with calibrator day 0 (CD45−EpCAM−CD31−pdpn− cells). Data are expressed as mean ± SD ($n = 6$). *$P < 0.05$; **$P < 0.01$; ***$P < 0.001$; one-way ANOVA. (*E*) Gene expression analysis for cxcl13, ccl19, and baff transcripts on fibroblast subsets sorted on differential ICAM-1 and VCAM-1 expression. Relative quantitation (RQ) was calculated with calibrator as day 0 (CD45−EpCAM−CD31−ICAM-1−VCAM-1− cells). Data are expressed as mean ± SD ($n = 6$). *$P < 0.05$; ***$P < 0.001$; one-way ANOVA.
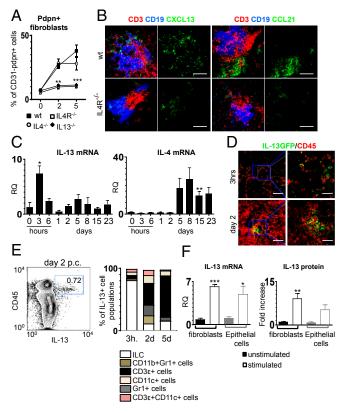
Fig. 3. The IL13 pathway is significantly involved in immunofibroblast activation. (*A*) Flow cytometry data of the percentage of pdpn⁺ stroma from wt (black squares, $n = 3$ to 6), IL4R⁻/⁻ (open squares, $n = 3$ to 6), IL4⁻/⁻ (open circles, $n = 3$ to 5) and IL13⁻/⁻ (black triangle, $n = 3$ to 5) mice at days 0, 2, and 5 p.c. **$P < 0.01$; ***$P < 0.001$; one-way ANOVA. Data are represented as mean ± SD. (*B*) Immunofluorescence of lymphoid aggregates in salivary glands (day 15 p.c.) from wt and IL4R⁻/⁻ mice (CD3, red; CD19, blue; CXCL13 or CCL21, green). (Scale bars: 100 μm.) (*C*) il13 and il4 transcripts time course analysis by qRT-PCR in wt mice. Data are represented as mean ± SD of 2 to 3 independent experiments with 2 to 3 mice per group. *$P < 0.05$; **$P < 0.01$; one-way ANOVA. (*D*) Immunofluorescence staining for IL13 (green) and CD45 (red) at 3 h and day 2 p.c. (Scale bars: 50 μm; *Inset* shows higher magnification, scale bars: 10 μm.) (*E*) Identification of IL13⁺ cells in the CD45⁺ compartment by flow cytometry at 3 h and days 2 and 5 p.c. (*F*) Analysis of IL13 transcript and protein expression by fibroblasts ($n = 3$) and epithelial cells ($n = 3$). *$P < 0.05$; **$P < 0.01$; ***$P < 0.001$; t test. Data are represented as mean ± SD.

express IL22Rα, and this expression increases significantly in pdpn⁺ cells upon viral infection (Fig. 4 *A* and *B*). To test the proliferative ability of IL22, we administered recombinant murine (m) IL22 to unmanipulated salivary glands in vivo and also in vitro to isolated pdpn⁺ fibroblasts. We observed that IL22 was sufficient to induce proliferation of pdpn⁺ cells both when administered in vivo (Fig. 4C) and in vitro (Fig. 4D). Correspondingly, both IL22- and IL22R-deficient mice presented a numeric defect in pdpn⁺ stromal cells that was significant from day 5 postinfection (Fig. 4E). This defect was accompanied by a significant decrease in BrdU incorporation by the fibroblasts (Fig. 4F) and could be reproduced by administering therapeutic doses of the anti-IL22 antibody to virus-cannulated wt mice (Fig. 4G). Together, these data suggest that, during TLS assembly, while IL13 mediates the early acquisition of an "activated phenotype" of the resident progenitors, IL22 is responsible for the expansion of this immunofibroblast network.

Priming and Expansion of pdpn⁺ Fibroblasts in TLS Are Independent of LTα1β2 and RORγ⁺ Cells. Full development of FRCs in SLOs is largely regulated by LTα1β2, provided during embryogenesis by

RORγ⁺ lymphoid tissue inducer cells[21]. To investigate the effects that LTα1β2 and RORγ exert on the identified population of immunofibroblasts, we induced salivary gland inflammation in Ltβr⁻/⁻ and Rorγ⁻/⁻ mice. Both strains exhibited normal up-regulation of ICAM-1, VCAM-1, and pdpn and normal proliferation of the pdpn⁺ fibroblasts up to day 8 p.c. (Fig. 5A and *SI Appendix*, Fig. S5). Interestingly, by day 15 p.c., both strains exhibited a defect in the number and proliferation of pdpn⁺ fibroblasts, together with a
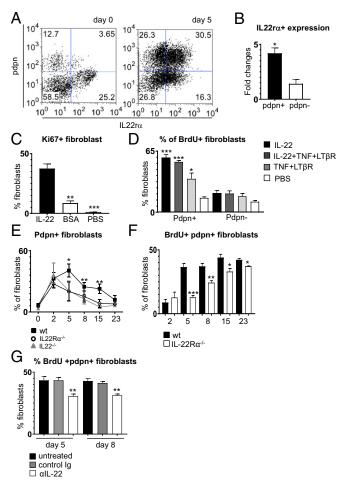

Fig. 4. Expansion of immunofibroblasts is dependent on the IL22/IL22Rα pathway. (*A*) Representative plot of IL22Rα expression by CD45⁻EpCAM⁻CD31⁻ cells at days 0 and 5 p.c. (*B*) Fold change of IL22Rα expression by pdpn⁺ ($n = 3$) and pdpn⁻ ($n = 3$) fibroblasts, analyzed by flow cytometry. *$P < 0.05$; paired t test. (*C*) Flow cytometry analysis of Ki67⁺pdpn⁺ fibroblasts in wt salivary glands cannulated with IL22 (black bars), BSA (white bars), or PBS (gray bars) and analyzed at day 2 p.c. Data are represented as mean ± SD of 3 independent experiments, 2 mice per group. **$P < 0.01$; ***$P < 0.001$; one-way ANOVA. (*D*) Percentage of BrdU incorporation in pdpn⁺ fibroblasts isolated from wt salivary glands at day 2 p.c. and then stimulated in vitro with IL22 (black bars); with IL22, TNFα, and LTβR agonist (dark gray bars); with TNFα and LTβR agonist (light gray bars); or with PBS (white bars). Data are represented as mean ± SD of 2 independent experiments, *$P < 0.05$; ***$P < 0.001$; one-way ANOVA. (*E*) Percentage of pdpn⁺ fibroblasts in IL22Rα⁻/⁻ (open circles, $n = 4$ to 6), IL22⁻/⁻ (gray triangles, $n = 4$ to 6), and wt mice (black squares, $n = 3$ to 6). *$P < 0.05$; **$P < 0.01$; one-way ANOVA. Data are represented as mean ± SD. (*F*) Analysis of BrdU incorporation by pdpn⁺ fibroblast from wt (black bars, $n = 4$ to 6) and IL22Rα⁻/⁻ (white bars, $n = 3$ to 5) mice (days 2, 5, 8, 15, and 23 p.c.). *$P < 0.05$; **$P < 0.01$; ***$P < 0.001$; one-way ANOVA. Data are represented as mean ± SD. (*G*) Analysis of BrdU⁺ pdpn⁺ fibroblasts at days 5 and 8 p.c. with anti-IL22 (open bars), control Ig (gray bars), or untreated (black bars). Data are presented as the mean ± SD of 2 independent experiments, with 2 to 3 mice per group. **$P < 0.01$; one-way ANOVA.

reduction in the percentage of the ICAM-1/VCAM-1 intermediate and high cells (Fig. 5A and SI Appendix, Fig. S5).

During TLS assembly, Ltβr$^{-/-}$ and Rorγ$^{-/-}$ mice failed to express normal levels of lymphoid chemokines and to form organized foci upon viral infection (Fig. 5 B–E). These data suggest that, while not required for priming and expansion of the fibroblastic network, Ltα1β2- and Rorγ-positive cells play a nonredundant role at the final differentiation and stabilization of the functional phenotype of the immunofibroblasts.

Lymphocytes Are Dispensable for pdpn$^+$ Fibroblast Priming but Required for Expansion and Conversion of the Stromal Network to a Fully Mature Immune Phenotype. The data generated suggested that different phases of fibroblast modifications during TLS assembly are regulated by diverse cytokines and depend on the interaction between fibrobla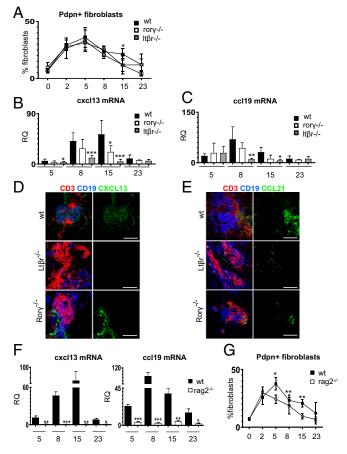sts and different cell types. To better understand this phenomenon, we induced TLS formation in lymphocyte-deficient mice. As expected, Rag2$^{-/-}$ mice infected with adenovirus failed to induce homeostatic chemokine expression and exhibited a phenotype similar to that of LtβR$^{-/-}$ mice (Fig. 5F). However, the analysis of the fibroblast compartment in Rag2$^{-/-}$ mice showed an early significant defect in the expansion of the pdpn$^+$ fibroblasts, not observed in the absence of the LTβR signal. This defect was significant from day 5 post viral infection (Fig. 5G) and closely mimicked the phenotype observed in the IL22R$^{-/-}$ and IL22$^{-/-}$ mice (Fig. 4). Interestingly, the early fibroblast priming was maintained in Rag2$^{-/-}$ (Fig. 5G), confirming that IL13 expression and the engagement of IL4R in the salivary gland at this stage is not dependent on lymphocytes. Accordingly, PCR analysis for IL13 in the Rag2$^{-/-}$ demonstrated a conserved signal for this cytokine (SI Appendix, Fig. S5).

Deletion of pdpn$^+$/Fap$^+$ Fibroblasts Abrogates TLS Establishment and Compromises Establishment of Local Pathology. To finally demonstrate whether the fibroblast network that we described in vivo is required for TLS assembly and maintenance in vivo, we utilized the Dm2 mouse to deplete pdpn-expressing cells. Dm2 mice have been previously used to delete pdpn$^+$ FRCs in SLOs, taking advantage of the expression of FAP$^+$ on pdpn$^+$ FRCs and the engineered expression of the diphtheria receptor (DTR) under the FAP promoter (5, 24, 25).

We firstly demonstrated that, similarly to SLOs, pdpn$^+$ cells in the TLS forming in both wt mice and Dm2 salivary glands express FAP (Fig. 6 A and B) and that FAP expression is upregulated upon inflammation in viral-infected salivary glands (Fig. 6 C and D). We then treated Dm2 mice with diptheria toxin as previously described (5, 24, 25) before the induction of TLS (Materials and Methods). By day 8 postinfection in Dm2$^+$, but not in control treated mice, there was a significant loss of pdpn$^+$ stromal cells in the salivary gland (Fig. 6E and SI Appendix, Fig. S6); this effect was associated with a reduced number of lymphocytes (Fig. 6F and SI Appendix, Fig. S5), less organized TLS (Fig. 6G and SI Appendix, Fig. S6), and low chemokine expression in infected glands (Fig. 6H). Local disaggregation of TLS resulted in abrogated autoantibody production (Fig. 6I). Given the potential interference of FAP systemic deletion on the immune response (5), we performed local deletion of FAP$^+$ cells by delivering DTX directly in the salivary glands. Infected mice treated with local DTX also display loss of pdpn$^+$ fibroblasts and a decrease in CD45$^+$ cells, activated T cells, and B cells (SI Appendix, Fig. S6). Overall, local stromal cell depletion was less efficient than systemic and was reflected in the lack of impact on ANA production in treated mice.

Discussion

TLS form in response to the immunological requirement to generate a local immune response against invading pathogens and local antigens (26). However, TLS persistence in autoimmune conditions correlates with worse outcome, including the development of MALT (mucosal-associated lymphoid tissue) lymphoma and increased systemic manifestations (1). Resistance to immune-cell depletion in subsets of patients with TLS-associated autoimmune conditions has been linked to the inability to interfere with local excess of survival factors and cytokines produced within the TLS. This suggests that the identification of the molecular mechanisms responsible for the establishment and maintenance of this local microenvironment could be exploited therapeutically (2). Here, we demonstrate that TLS assembly, both in humans and in an animal model of TLS, is underpinned by the formation of a network of pdpn$^+$ immunofibroblasts, phenotypically and functionally similar to the FRC networks described within SLOs. Interestingly, murine and human fibroblasts display differential associations

Fig. 5. LTα1β2 and RORγ$^+$ cells regulate chemokine expression but not early fibroblast priming or expansion. (A) Time course flow cytometry analysis of the percentage of pdpn$^+$ fibroblasts from wt (black squares, n = 3 to 5), Rorγ$^{-/-}$ (open squares, n = 3 to 5), and Ltβr$^{-/-}$ (gray squares, n = 3 to 5) mice. *P < 0.05; one-way ANOVA. Data are represented as mean ± SD. (B and C) Analysis of cxcl13 and ccl19 mRNA transcripts by qRT-PCR in wt (black bars, n = 7 to 12), Rorγ$^{-/-}$ (open bars, n = 4 to 5), and Ltβr$^{-/-}$ (gray bars, n = 4 to 7) mice at days 5, 8, 15, and 23 p.c. *P < 0.05; **P < 0.01; ***P < 0.001; one-way ANOVA. Data are represented as mean ± SD. (D and E) Immunofluorescence of salivary glands (day 15 p.c.) from wt, Ltβr$^{-/-}$, and Rorγ$^{-/-}$ mice [CD3, red; CD19, blue; CXCL13 (D) or CCL21 (E), green]. (Scale bars: 100 μm.) (F) qRT-PCR analysis of cxcl13 and ccl19 mRNA from wt (black bars, n = 4 to 6) and Rag2$^{-/-}$ (white bars, n = 4 to 6) salivary glands at days 5, 8, 15, and 23 p.c. *P < 0.05; **P < 0.01; ***P < 0.001; one-way ANOVA. Data are represented as mean ± SD. (G) Time course flow cytometry analysis of the percentage of pdpn$^+$ fibroblasts from wt (black squares, n = 4 to 6) and Rag2$^{-/-}$ (open squares, n = 4 to 6) mice. *P < 0.05; **P < 0.01; one-way ANOVA. Data are represented as mean ± SD.
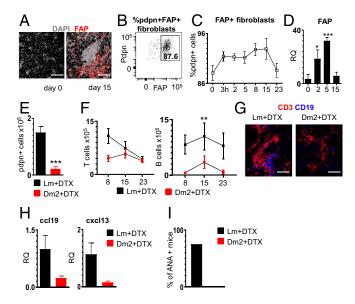
Fig. 6. Depletion of FAP[+] fibroblasts impairs the formation of TLS. (*A*) Immunofluorescence staining of FAP (red) and DAPI (gray) in wt salivary glands at days 0 and 15 p.c. (Scale bars: 200 μm.) (*B*) Representative flow cytometry plot of FAP expression by pdpn[+] fibroblasts. The gate shows percentage of FAP+ pdpn+ cells. (*C*) Time course analysis of the percentage of pdpn[+] FAP[+] fibroblasts in wt mice. Data are presented as mean ± SD. (*D*) Analysis of fap mRNA transcript by qRT-PCR in wt salivary glands at days 0, 2, 5, and 15 p.c. (*n* = 4 to 9). *$P < 0.05$; ***$P < 0.001$; one-way ANOVA. Data are represented as mean ± SD. (*E*) Flow cytometry data for absolute numbers of pdpn[+] fibroblasts at day 8 p.c. in Lm DTX treated (black bars, *n* = 8) and Dm2 DTX treated (red bars, *n* = 6). ***$P < 0.001$; *t* test. Data are represented as mean ± SD. (*F*) Flow cytometry data for absolute numbers of T and B lymphocytes at days 8, 15, and 23 p.c. in Lm DTX treated (black squares) and Dm2 DTX treated (red bars). Data are represented as mean ± SD of 2 independent experiments with at least 3 mice for each experiment. **$P < 0.01$; one-way ANOVA. (*G*) Immunofluorescence staining of CD3 (red) and CD19 (blue) in Lm DTX treated and Dm2 DTX treated at day 8 p.c. (Scale bars: 100 μm.) (*H*) qRT-PCR analysis of cxcl13 and ccl19 mRNA from Lm DTX treated (black bars, *n* = 6) and Dm2 DTX treated (red bars, *n* = 4) salivary glands at day 8 p.c. Data are represented as mean ± SD. (*I*) Percentage of positive mice for ANA in lm DTX treated (black bar) and Dm2 DTX treated (red bar) experimental groups at day 23 p.c.

between expression of chemokines and survival factors and expression of ICAM-1, VCAM-1, and CD34. The developmental imprinting underpinning these differences is currently under investigation.

The cellular requirements and microenvironmental signals responsible for the formation of this fibroblast network, both in humans and mice, appear to be conserved across species and unique to TLS and encompass the engagement of Th2 cytokines and IL22, in synergy with LTα1β2. The analysis of this cascade and the cellular interaction responsible for it demonstrates that lymphocytes are dispensable for the early priming of the immunofibroblast progenitors in TLS. Lymphocytes are, however, required for the expansion of the network and for its full conversion to an immune phenotype.

Genome-wide association studies have previously identified MHC class II haplotypes and components of the IL4/IL13 receptor complex, including Tyk2, as independent risk factors in immune-mediated inflammatory diseases (27, 28). This risk was classically associated with the role of the IL4R pathway in CD4 T cell function. However, MHC class II, the IL4/IL13 receptor complex, and Tyk2 expression are expressed and functional in nonhematopoietic cells, including smooth muscle cells. Moreover, IL4R activation is known to regulate adult muscle regeneration (29). Previous reports have suggested the association between IL13 and the production of autoantibodies (17–22). Nevertheless,

no functional proof of this relationship has been provided outside the role of this pathway in B and T cell regulation (30). Here, we demonstrate that the release of IL13 by resident ILCs and stromal cells, including fibroblasts and epithelium, directly regulates phenotypical changes but not proliferation of a population of pdpn[+] immunofibroblast progenitors. This IL4R-mediated priming is required for the up-regulation of adhesion molecules, in particular VCAM-1, that enable the interaction of the fibroblasts with incoming leukocytes. IL13 production by resident stromal cells strongly assimilates this intrinsic and rapid response with the mechanisms of immunosurveillance ascribed to this cytokine in carcinogenesis (31). In this latter model, IL13 regulated the release of thymic stromal lymphopoietin and IL33, thereby accelerating epithelium repair (31). In our example, IL13 acts on a resident population of fibroblasts, modulating their ability to interact with incoming immune cells and form TLS. Together, these observations provide evidence in support of a critical role of IL13 in response to external danger signals in a series of pathogenic settings that extend from inflammation to autoimmunity and cancer.

Intriguingly, IL4R engagement was not able to induce fibroblast proliferation. FRC expansion postimmunization has been described in SLOs and deemed dependent on LTα1β2 and IL4R (32–34). Here, we demonstrate that, in TLS, expansion of pdpn[+] fibroblasts also occurs, with active stromal cell proliferation peaking at day 5 postinfection. However, this phenomenon is largely independent of LTα1β2 and RORγt^{+} cells, but regulated by lymphocytes and IL22, a cytokine known to promote stromal cell repair and proliferation (35–38). The biological effect described here in murine and human fibroblasts, together with our previous report on the link between IL22 and CXCL13 expression in TLS, strongly advocates for an intervention against this cytokine in clinical practice.

Interestingly, RORγt-dependent IL17 production appears not to play a major role in this system as a fairly conserved expansion of the immunofibroblasts occurs, along with TLS formation in RORγt^{−/−} mice. Whether this is a feature specific of the TLS forming at mucosal sites is not clear as IL17 production has been deemed important for TLS establishment in other organs (13–15).

We previously demonstrated that interfering in vivo with IL22 expression by the use of a blocking antibody profoundly affects TLS maintenance in the tissue (12). Here, we expanded this observation and reported the formation of aberrant TLS with decreased immunofibroblast proliferation in mice treated with anti-IL22 antibodies, but also in mice deficient for IL4R and in a model of fibroblast depletion in vivo (Dm2). Previous work demonstrated that stromal cell depletion in SLOs of Dm2 mice only marginally affects lymphoid organ architecture (5). However, the impact on immune effector functions of Dm2 mice with diphtheria toxin demonstrates that systemic depletion of immunofibroblasts in TLS exerts a more profound effect, severely compromising aggregate assembly, inducing loss of anatomical organization, diminishing lymphocyte recruitment, and resolution of tissue pathology. Importantly, in this model and, similarly, in the absence of the IL4R or IL22R signaling, a reduction in the production of antinuclear antibodies was observed. These observations highlight the importance of a normal fibroblast network to support autoantibody production. Stromal cell depletion, induced by local DTX delivery, was less efficient in depleting immunofibroblasts. However, it still profoundly affected local pathology, but not systemic ANA production in viral infected animals.

Several reports have highlighted the association between failure to respond to B cell-depleting therapies and the persistence of TLS in the tissue of patients with autoimmune conditions (39–47). These observations establish a pathogenic role for TLS and their local microenvironment to sustain pathology. Here, we have demonstrated that the formation of a network of immune fibroblasts in TLS is responsible for the establishment of

the TLS pathogenic microenvironment and that interfering with the signals responsible for its establishment profoundly affects local pathology and interferes with autoantibody production, providing a strong rationale for targeting immunofibroblasts in the treatment of TLS-associated diseases.

Materials and Methods

Study Design. Immunohistochemistry, immunofluorescence (IF), and flow cytometry were used to define the phenotype of immunofibroblasts in the salivary glands of patients with pSS. Tissue was obtained from patients recruited in the OASIS cohort (Optimising assessments in Sjögren's syndrome) at University of Birmingham under ethics no. 10-018.

IL13, IL4, and IL22 receptor expression was detected in both humans and mice, and differential biological effects were observed in fibroblasts stimulated with these molecules. To dissect these effects in vivo, we studied the dynamic response of a population of pdpn$^+$ cells in a model of TLS assembly in wt mice and in mutants defective for IL13, IL4R, IL4, IL22, IL22R, LTβR, and Rorγ, as well as Rag2 mice. Mice were maintained in the Biomedical Service Unit at the University of Birmingham according to Home Office and local ethics committee regulations (University of Birmingham), under license no. P4B291FAA. IF, flow cytometry, and qRT PCR were used to assess differential effects in these mutants in the salivary glands of mice killed at different time points. Recombinant proteins for the molecules of interest and a blocking antibody against IL22 were used in gain- or loss-of-function experiments to dissect the requirements of these pathways in fibroblast maturation and TLS formation. Finally, to prove the effect that pdpn$^+$ fibroblast deletion would exert on TLS, we used DM2 mice that express the diphtheria toxin receptor under the FAP promoter.

Detailed materials and methods can be found in *SI Appendix*.

1. C. Pitzalis, G. W. Jones, M. Bombardieri, S. A. Jones, Ectopic lymphoid-like structures in infection, cancer and autoimmunity. *Nat. Rev. Immunol.* **14**, 447–462 (2014).
2. F. Barone et al., Stromal fibroblasts in tertiary lymphoid structures: A novel target in chronic inflammation. *Front. Immunol.* **7**, 477 (2016).
3. C. D. Buckley, F. Barone, S. Nayar, C. Bénézech, J. Caamaño, Stromal cells in chronic inflammation and tertiary lymphoid organ formation. *Annu. Rev. Immunol.* **33**, 715–745 (2015).
4. L. B. Rodda et al., Single-cell RNA sequencing of lymph node stromal cells reveals niche-associated heterogeneity. *Immunity* **48**, 1014–1028.e6 (2018).
5. A. E. Denton, E. W. Roberts, M. A. Linterman, D. T. Fearon, Fibroblastic reticular cells of the lymph node are required for retention of resting but not activated CD8+ T cells. *Proc. Natl. Acad. Sci. U.S.A.* **111**, 12139–12144 (2014).
6. M. Novkovic, L. Onder, G. Bocharov, B. Ludewig, Graph theory-based analysis of the lymph node fibroblastic reticular cell network. *Methods Mol. Biol.* **1591**, 43–57 (2017).
7. M. Novkovic et al., Topological small-world organization of the fibroblastic reticular cell network determines lymph node functionality. *PLoS Biol.* **14**, e1002515 (2016).
8. C. Bénézech et al., Ontogeny of stromal organizer cells during lymph node development. *J. Immunol.* **184**, 4521–4530 (2010).
9. T. Cupedo, G. Kraal, R. E. Mebius, The role of CD45+CD4+CD3- cells in lymphoid organ development. *Immunol. Rev.* **189**, 41–50 (2002).
10. G. Eberl, D. R. Littman, The role of the nuclear hormone receptor RORgammat in the development of lymph nodes and Peyer's patches. *Immunol. Rev.* **195**, 81–90 (2003).
11. L. Peduto et al., Inflammation recapitulates the ontogeny of lymphoid stromal cells. *J. Immunol.* **182**, 5789–5799 (2009).
12. F. Barone et al., IL-22 regulates lymphoid chemokine production and assembly of tertiary lymphoid organs. *Proc. Natl. Acad. Sci. U.S.A.* **112**, 11024–11029 (2015).
13. A. Peters et al., Th17 cells induce ectopic lymphoid follicles in central nervous system tissue inflammation. *Immunity* **35**, 986–996 (2011).
14. N. B. Pikor et al., Integration of Th17- and lymphotoxin-derived signals initiates meningeal-resident stromal cell remodeling to propagate neuroinflammation. *Immunity* **43**, 1160–1173 (2015).
15. J. Rangel-Moreno et al., The development of inducible bronchus-associated lymphoid tissue depends on IL-17. *Nat. Immunol.* **12**, 639–646 (2011).
16. A. Link et al., Association of T-zone reticular networks and conduits with ectopic lymphoid tissues in mice and humans. *Am. J. Pathol.* **178**, 1662–1675 (2011).
17. A. Spadaro, T. Rinaldi, V. Riccieri, E. Taccari, G. Valesini, Interleukin-13 in autoimmune rheumatic diseases: Relationship with the autoantibody profile. *Clin. Exp. Rheumatol.* **20**, 213–216 (2002).
18. J. Mahlios, Y. Zhuang, Contribution of IL-13 to early exocrinopathy in Id3-/- mice. *Mol. Immunol.* **49**, 227–233 (2011).
19. Z. Xu, Y. Chen, Determination of serum interleukin-13 and nerve growth factor in patients with systemic lupus erythematosus and clinical significance. *J. Huazhong Univ. Sci. Technolog. Med. Sci.* **25**, 360–361 (2005).
20. G. M. Villarreal, J. Alcocer-Varela, L. Llorente, Differential interleukin (IL)-10 and IL-13 gene expression in vivo in salivary glands and peripheral blood mononuclear cells from patients with primary Sjögren's syndrome. *Immunol. Lett.* **49**, 105–109 (1996).
21. D. I. Mitsias et al., The Th1/Th2 cytokine balance changes with the progress of the immunopathological lesion of Sjogren's syndrome. *Clin. Exp. Immunol.* **128**, 562–568 (2002).
22. K. Raza et al., Early rheumatoid arthritis is characterized by a distinct and transient synovial fluid cytokine profile of T cell and stromal cell origin. *Arthritis Res. Ther.* **7**, R784–R795 (2005).
23. M. Bombardieri et al., Inducible tertiary lymphoid structures, autoimmunity, and exocrine dysfunction in a novel model of salivary gland inflammation in C57BL/6 mice. *J. Immunol.* **189**, 3767–3776 (2012).
24. D. T. Fearon, The carcinoma-associated fibroblast expressing fibroblast activation protein and escape from immune surveillance. *Cancer Immunol. Res.* **2**, 187–193 (2014).
25. M. Kraman et al., Suppression of antitumor immunity by stromal cells expressing fibroblast activation protein-alpha. *Science* **330**, 827–830 (2010).
26. G. W. Jones, S. A. Jones, Ectopic lymphoid follicles: Inducible centres for generating antigen-specific immune responses within tissues. *Immunology* **147**, 141–151 (2016).
27. M. Ban et al.; Wellcome Trust Case-Control Consortium (WTCCC), Replication analysis identifies TYK2 as a multiple sclerosis susceptibility factor. *Eur. J. Hum. Genet.* **17**, 1309–1313 (2009).
28. P. D. Burbelo, K. Ambatipudi, I. Alevizos, Genome-wide association studies in Sjögren's syndrome: What do the genes tell us about disease pathogenesis? *Autoimmun. Rev.* **13**, 756–761 (2014).
29. J. E. Heredia et al., Type 2 innate signals stimulate fibro/adipogenic progenitors to facilitate muscle regeneration. *Cell* **153**, 376–388 (2013).
30. T. A. Wynn, IL-13 effector functions. *Annu. Rev. Immunol.* **21**, 425–456 (2003).
31. T. Dalessandri, G. Crawford, M. Hayes, R. Castro Seoane, J. Strid, IL-13 from intraepithelial lymphocytes regulates tissue homeostasis and protects against carcinogenesis in the skin. *Nat. Commun.* **7**, 12080 (2016).
32. C. Y. Yang et al., Trapping of naive lymphocytes triggers rapid growth and remodeling of the fibroblast network in reactive murine lymph nodes. *Proc. Natl. Acad. Sci. U.S.A.* **111**, E109–E118 (2014).
33. L. K. Dubey et al., Lymphotoxin-dependent B cell-FRC crosstalk promotes de novo follicle formation and antibody production following intestinal helminth infection. *Cell Rep.* **15**, 1527–1541 (2016).
34. L. K. Dubey, P. Karempudi, S. A. Luther, B. Ludewig, N. L. Harris, Interactions between fibroblastic reticular cells and B cells promote mesenteric lymph node lymphangiogenesis. *Nat. Commun.* **8**, 367 (2017).
35. S. Pantelyushin et al., Rorγt+ innate lymphocytes and γδ T cells initiate psoriasiform plaque formation in mice. *J. Clin. Invest.* **122**, 2252–2256 (2012).
36. A. Andoh et al., Interleukin-22, a member of the IL-10 subfamily, induces inflammatory responses in colonic subepithelial myofibroblasts. *Gastroenterology* **129**, 969–984 (2005).
37. M. Colonna, Interleukin-22-producing natural killer cells and lymphoid tissue inducer-like cells in mucosal immunity. *Immunity* **31**, 15–23 (2009).
38. J. A. Dudakov, A. M. Hanash, M. R. van den Brink, Interleukin-22: Immunobiology and pathology. *Annu. Rev. Immunol.* **33**, 747–785 (2015).
39. F. Barone, S. Colafrancesco, Sjögren's syndrome: From pathogenesis to novel therapeutic targets. *Clin. Exp. Rheumatol.* **34** (suppl. 98), 58–62 (2016).
40. F. Lavie et al., Increase of B cell-activating factor of the TNF family (BAFF) after rituximab treatment: Insights into a new regulating system of BAFF production. *Ann. Rheum. Dis.* **66**, 700–703 (2007).
41. S. De Vita et al., Sequential therapy with belimumab followed by rituximab in Sjögren's syndrome associated with B-cell lymphoproliferation and overexpression of BAFF: Evidence for long-term efficacy. *Clin. Exp. Rheumatol.* **32**, 490–494 (2014).
42. L. Quartuccio et al., Controversies on rituximab therapy in sjögren syndrome-associated lymphoproliferation. *Int. J. Rheumatol.* **2009**, 424935 (2009).
43. L. Quartuccio et al., Resistance to rituximab therapy and local BAFF overexpression in Sjögren's syndrome-related myoepithelial sialadenitis and low-grade parotid B-cell lymphoma. *Open Rheumatol. J.* **2**, 38–43 (2008).
44. B. Marston, A. Palanichamy, J. H. Anolik, B cells in the pathogenesis and treatment of rheumatoid arthritis. *Curr. Opin. Rheumatol.* **22**, 307–315 (2010).
45. S. Bugatti, B. Vitolo, R. Caporali, C. Montecucco, A. Manzo, B cells in rheumatoid arthritis: From pathogenic players to disease biomarkers. *BioMed Res. Int.* **2014**, 681678 (2014).
46. C. Gorman, M. Leandro, D. Isenberg, B cell depletion in autoimmune disease. *Arthritis Res. Ther.* **5** (suppl. 4), S17–S21 (2003).
47. G. Nocturne, X. Mariette, B cells in the pathogenesis of primary Sjögren syndrome. *Nat. Rev. Rheumatol.* **14**, 133–145 (2018).

IMMUNOLOGY AND INFLAMMATION